

Primordial Black Holes as Seeds for Extremely Overmassive AGN Observed by JWST

SAIYANG ZHANG (張賽陽) ^{1,2} BOYUAN LIU (劉博遠) ^{3,4} VOLKER BROMM ^{2,5} AND FLORIAN KÜHNEL ^{6,7}

¹*Department of Physics, University of Texas at Austin, Austin, TX 78712, USA*

²*Weinberg Institute for Theoretical Physics, Texas Center for Cosmology and Astroparticle Physics,
University of Texas at Austin, Austin, TX 78712, USA*

³*Institute of Astronomy, University of Cambridge, Madingley Road, Cambridge, CB3 0HA, UK*

⁴*Universität Heidelberg, Zentrum für Astronomie, Institut für Theoretische Astrophysik, D-69120 Heidelberg, Germany*

⁵*Department of Astronomy, University of Texas at Austin, Austin, TX 78712, USA*

⁶*Max-Planck-Institut für Physik, Boltzmannstr. 8, 85748 Garching, Germany*

⁷*Arnold Sommerfeld Center, Ludwig-Maximilians-Universität, Theresienstr. 37, 80333 München, Germany*

ABSTRACT

The James Webb Space Telescope (JWST) has recently identified Abell 2744–QSO1 as a compact, metal-poor, black hole (BH) dominated galaxy at $z \simeq 7$. This system exhibits an extreme black-hole-to-stellar mass ratio and unusually low metallicity, posing significant challenges to BH seeding models. Motivated by these discoveries, we perform high-resolution cosmological simulations with a massive primordial black hole (PBH; $M_{\text{BH}} = 5 \times 10^7 M_{\odot}$) seed, incorporating for the first time a fully coupled treatment of PBH accretion, BH feedback, and Population III/II star formation and stellar feedback. Although PBHs accelerate structure formation through the seed effect, the associated strong thermal feedback from the accretion delays the onset of star formation to $z \lesssim 10$, producing short, bursty episodes throughout the subsequent evolution. PBH-driven outflows expel enriched gas from the nucleus, while sustained inflows from the intergalactic medium continuously replenish pristine material. This feedback-regulated cycle naturally yields low accretion rates ($\dot{m}_{\text{BH}}/\dot{m}_{\text{edd}} \sim 1 - 10\%$), subsolar metallicities ($Z/Z_{\odot} \lesssim 10^{-2}$) and extreme M_{BH}/M_{\star} ratios during both the initial star-forming phase and the subsequent quenching phases, in excellent agreement with JWST observations. Our results demonstrate that massive PBHs offer a viable pathway for forming the most extreme high-redshift systems, providing a physically motivated explanation for the extraordinary properties of Abell 2744–QSO1, as a sub-class of the broader population of JWST-discovered “little red dots”.

Keywords: Dark matter (353) — Early universe (435) — Galaxy formation (595) — Population III stars (1285) — Supermassive black holes (1663)

1. INTRODUCTION

Since the launch of the *James Webb Space Telescope* (JWST), an unexpected population of massive supermassive black holes (SMBHs) has been revealed at very high redshifts ($z \gtrsim 7$) (e.g., A. D. Goulding et al. 2023; R. L. Larson et al. 2023; Á. Bogdán et al. 2024; J. E. Greene et al. 2024; O. E. Kovács et al. 2024; R. Maiolino et al. 2024; P. Natarajan et al. 2024; L. Napolitano et al. 2025). Among these early systems, a class of compact, extremely red, and spectroscopically peculiar sources, commonly referred to as “little red dots” (LRDs), has emerged as a distinct population (e.g., I. Labbé et al.

2023; V. Kokorev et al. 2024; G. C. K. Leung et al. 2025; D. D. Kocevski et al. 2025; A. J. Taylor et al. 2025; I. Labbé et al. 2025). These newly-discovered objects are found to host central black holes (BHs) that are often ‘overmassive’ relative to their stellar components, with black-hole-to-stellar mass ratios exceeding the local relation (e.g. F. Pacucci et al. 2023; K. Inayoshi et al. 2024). Among those discoveries, one of the most striking examples is the JWST source Abell 2744–QSO1, whose inferred BH mass ($M_{\text{BH}} \sim 5 \times 10^7 M_{\odot}$), lack of significant stellar contributions in its kinematics and spectra ($M_{\star} \lesssim 2 \times 10^7 M_{\odot}$), combined with extremely low metallicity ($Z \lesssim 0.01 Z_{\odot}$) and low accretion efficiency ($f_{\text{Edd}} \sim 0.01 - 0.03$) at $z \sim 7$ pose severe challenges to conventional models of SMBH formation and coevolu-

tion with its host galaxy (L. J. Furtak et al. 2023; X. Ji et al. 2025; R. Maiolino et al. 2025; I. Juodžbalis et al. 2025).

Traditional light-seed scenarios, typically related to stellar remnants of Population III (Pop III) stars (see reviews in, e.g., A. Smith & V. Bromm 2019; K. Inayoshi et al. 2020), struggle to reproduce both the high inferred accretion rates and the black-hole-to-stellar mass ratios implied by JWST observations (e.g., M. Milosavljević et al. 2009; J. Jeon et al. 2023; Á. Bogdán et al. 2024). These models generally require sustained super-Eddington accretion over extended periods (e.g., T. Alexander & P. Natarajan 2014; J. Jeon et al. 2025a). An alternative pathway is the formation of massive BHs through the direct collapse of pristine, metal-poor gas with minimal fragmentation (A. Loeb & F. A. Rasio 1994; V. Bromm & A. Loeb 2003; M. C. Begelman et al. 2006; G. Lodato & P. Natarajan 2006). Such conditions typically demand a nearby source of intense soft-UV, Lyman–Werner (LW) radiation to suppress molecular hydrogen cooling (e.g., B. Agarwal et al. 2014; M. Habouzit et al. 2016; H. O’Brennan et al. 2025), which is absent in the vicinity of Abell 2744–QSO1 (I. Juodžbalis et al. 2025).

Another explanation involves the presence of *primordial black holes* (PBHs) that predate galaxy formation (for analytical work see, e.g., N. Düchting 2004; J. L. Bernal et al. 2018; V. De Luca et al. 2023; P. Dayal 2024; V. De Luca et al. 2025)⁸. PBHs, hypothesized to form from the collapse of density fluctuations shortly after the Big Bang (Y. B. Zel’dovich & I. D. Novikov 1967; S. Hawking 1971; B. J. Carr 1975; K. M. Belotsky et al. 2019; A. Escrivà 2022), may constitute only a small fraction of the dark matter, yet can profoundly influence cosmic evolution (for a review, see B. Carr & F. Kühnel 2020). On larger scales, depending on their mass spectrum and abundance, PBHs can enhance primordial density fluctuations and seed the formation of dark matter halos (e.g., K. J. Mack et al. 2007; M. Ricotti 2007; M. Ricotti et al. 2008; B. Carr & J. Silk 2018; D. Inman & Y. Ali-Haïmoud 2019; B.-Y. Su et al. 2023; P. E. Colazo et al. 2024; S. Zhang et al. 2024a), thus accelerating early structure formation (P. Meszaros 1975; N. Afshordi et al. 2003; A. Kashlinsky 2021; N. Cappelluti et al. 2022; B. Liu & V. Bromm 2022). Their early accretion can heat and ionize the intergalactic medium (IGM),

thus modifying cosmic radiation backgrounds (e.g., Y. Ali-Haïmoud & M. Kamionkowski 2017; V. De Luca et al. 2020; P. Lu et al. 2021; V. Takhistov et al. 2022; F. Ziparo et al. 2022; S. Zhang et al. 2024b; C. Casanueva-Villarreal et al. 2024), and potentially trigger the first episodes of star formation around PBH-seeded halos (B. Liu et al. 2022; B. Liu & V. Bromm 2023). Recent studies further suggest that massive PBHs ($\gtrsim 10^6 M_\odot$) can induce the formation of bound stellar clusters (S. Zhang et al. 2025a) or secondary massive BHs (S. Zhang et al. 2025b), giving rise to systems reminiscent of the LRDs discovered by JWST (P. Dayal & R. Maiolino 2025; A. Matheri et al. 2025). However, most previous simulations have included only BH accretion and feedback while ignoring stellar feedback (or vice versa), leaving open how PBHs coevolve with PBH-seeded galaxies in the early Universe.

In this work, we integrate the legacy stellar feedback model (J. Jaacks et al. 2018, 2019; B. Liu & V. Bromm 2020a,b) into our cosmological PBH simulation framework. This approach enables, for the first time, a combined treatment of both BH and stellar feedback in the early growth of PBH-seeded systems. Our simulations follow the coupled evolution of dark matter, baryons and stellar components from $z \simeq 1100$ to $z \simeq 7$, reproducing the physical conditions of Abell 2744–QSO1 and potentially other JWST LRDs, aiming to assess whether heavy PBH seeds can naturally account for the formation of these extreme high-redshift systems.

In Section 2, we describe the numerical setup for the simulation, focusing on the recipes for star formation and stellar feedback. From the simulated results, the detailed galaxy assembly and metal enrichment history around the central PBH is discussed in Section 3. The limitations and caveats are addressed in Section 4, and we present our conclusions in Section 5.

2. METHODOLOGY

The simulation is performed using the GIZMO code (P. F. Hopkins 2015), which couples the Lagrangian meshless finite-mass (MFM) hydrodynamics solver (with $N_{\text{ngb}} = 32$ neighbors) to the parallel Tree+PM gravity solver of GADGET-3 (V. Springel 2005). The non-equilibrium primordial chemistry and cooling network includes 12 species, following V. Bromm et al. (2002) and J. L. Johnson & V. Bromm (2006), supplemented by C II, O I, Si II and Fe II line cooling (J. Jaacks et al. 2018), with initial abundances at $z \simeq 1100$ set by D. Galli & F. Palla (2013). The *Planck18* cosmological parameters were adopted throughout (Planck Collaboration et al. 2020): $\Omega_{\text{m}} = 0.3111$, $\Omega_{\text{b}} = 0.04897$, $h = 0.6776$, $\sigma_8 = 0.8102$, $n_s = 0.9665$.

⁸ A few alternative formation scenarios have been proposed, such as core collapse of strongly self-interacting dark matter (e.g., F. Jiang et al. 2026) or direct collapse of gas at $z \gtrsim 100$ from the enhanced power spectrum at small scales (e.g., W. Qin et al. 2025)

Table 1. Summary of key parameters and main results. z_{ini} the initial redshift where the simulation starts, and N_{eff} the total number of particles within the simulation box of size $L = 1 h^{-1}$ Mpc. ϵ_r is the thermal coupling efficiency of BH feedback, $\langle f_{\text{edd}} \rangle \equiv \langle \dot{m}_{\text{BH}}/\dot{m}_{\text{edd}} \rangle$ is the time-averaged BH accretion rate in units of the Eddington limit, FULL_SF a flag to control whether we consider the full stellar feedback recipe or not, whereas ϵ_{DM} , ϵ_{gas} , and ϵ_* represent the (co-moving) softening lengths for PDM, gas, and stellar particles, respectively. Finally, z_{col} is the redshift when star formation begins around the central PBH, and M_* denotes the total mass of stars formed in the PBH-hosting halo, evaluated by the end of the simulation ($z \sim 7$).

Run	z_{ini}	N_{eff}	ϵ_r	$\langle f_{\text{edd}} \rangle$	FULL_SF	$\epsilon_{\text{DM}}[\text{kpc}/h]$	$\epsilon_{\text{gas}}[\text{kpc}/h]$	$\epsilon_*[\text{kpc}/h]$	z_{col}	$M_*[M_{\odot}]$
PBH_DMonly	3400	256^3	-	-	-	0.05	-	-	-	-
PBH_M5e7_fd005	1100	2×256^3	0.005	0.0076	✗	0.05	0.05	0.005	9.64	2.0×10^7
PBH_SF_M5e7_fd005	1100	2×256^3	0.005	0.0081	✓	0.05	0.05	0.005	8.20	7.7×10^5
PBH_SF_M5e7_fd0025	1100	2×256^3	0.0025	0.013	✓	0.05	0.05	0.005	8.58	3.2×10^5
PBH_SF_M5e7_fd01	1100	2×256^3	0.01	0.0047	✓	0.05	0.05	0.005	12.80	1.9×10^6

We describe the initial conditions and general numerical setup in Section 2.1, and the stellar formation and feedback prescriptions in Section 2.2. The relevant parameters for all runs are summarized in Table 1.

2.1. Initial Conditions

To reproduce the observed properties of Abell 2744–QSO1, we focus on the cosmic evolution surrounding an isolated PBH. The simulation box has a comoving side length of $L = 1 h^{-1}$ Mpc and contains $N_{\text{PDM}} = 256^3$ dark matter particles. The simulation begins at $z \simeq 3400$, where we place a BH of mass $5 \times 10^7 M_{\odot}$ at the center of the box⁹, generated using the MUSIC code (O. Hahn & T. Abel 2011). The numerical procedure for embedding the PBH and perturbing the surrounding particle dark matter (PDM) field is implemented using the PHANTOM code (S. Zhang et al. 2025), following the formalism in Y. Ali-Haïmoud & M. Kamionkowski (2017); D. Inman & Y. Ali-Haïmoud (2019); B. Liu et al. (2022); S. Zhang et al. (2024a), providing the initial condition for the PBH_DMonly run. We first evolve this run from $z \simeq 3400$ to the recombination epoch ($z \simeq 1100$) to establish the PDM distribution around the central PBH¹⁰. We then add a uniform baryonic component to initialize the full hydrodynamical

runs, resulting in a total of $N = 2 \times 256^3$ particles for both the PBH_SF_M5e7_fd005 and PBH_M5e7_fd005 runs with and without stellar feedback, respectively. The resulting gas and dark matter particle masses are $1.2 \times 10^3 M_{\odot}$ and $5.1 \times 10^3 M_{\odot}$.

BH accretion and feedback are modeled using the same subgrid prescription as in S. Zhang et al. (2025a) which self-consistently tracks the growth of the central PBH through Bondi-Hoyle-Lyttleton accretion with radiative/thermal feedback. The feedback is implemented by depositing energy into the surrounding gas according to a fiducial thermal radiation coupling efficiency of $\epsilon_r = \delta E_{\bullet, \text{inject}}/(L_{\bullet, \text{acc}} \delta t) = 0.005$ ¹¹, where $\delta E_{\bullet, \text{inject}}$ represents the thermal energy injected into the ambient medium, and $L_{\bullet, \text{acc}}$ is the accretion luminosity. Both runs are evolved from $z \simeq 1100$ to $z \simeq 7$, corresponding to the observed redshift of Abell 2744–QSO1 (X. Ji et al. 2025).

2.2. Star Formation and Stellar Feedback

During the simulation, when a gas particle becomes Jeans unstable near the central BH and survives for a free fall time, without being accreted by the BH or dispersed by feedback, it is converted into a stellar sink particle according to the star formation criterion of S. Zhang et al. (2025a). Our analysis focuses primarily on the PBH_SF_M5e7_fd005 run, which includes a physically

⁹ In this work, we simulate structure formation around an isolated PBH, motivated by the inferred mass of Abell 2744–QSO1 (I. Juodžbalis et al. 2025). The chosen box size limits the effective PBH mass fraction to $f_{\text{PBH}} \lesssim 8 \times 10^{-4}$, which is broadly compatible with formation scenarios based on early-Universe phase transitions (B. Carr et al. 2021a). However, such a massive PBH could also originate from mergers of initially clustered lower-mass PBHs (S. Zhang et al. 2024a; B. Zhang et al. 2025).

¹⁰ The PBH is treated as a freely moving collisionless particle providing the central gravitational potential; numerically, it is evolved like any other particle except for a boosted drag term during accretion to minimize BH wandering. To be specific, we apply a drag force $\vec{F} = -\dot{m}_{\text{edd}} \vec{v}_{\text{rel}}$ to the BH, given its Eddington accretion rate \dot{m}_{edd} and velocity \vec{v}_{rel} relative to gas. Consequently, the BH-gas relative velocity remains well below

the local sound speed throughout the simulation, rendering its contribution to the accretion rate subdominant.

¹¹ The adopted feedback coefficient is also chosen to reproduce the observed properties of the QSO-1 system, allowing for moderate star formation consistent with its inferred stellar content. We have also included two additional runs ($\epsilon_r = 0.0025$, PBH_SF_M5e7_fd0025 and $\epsilon_r = 0.01$, PBH_SF_M5e7_fd01) by varying this parameter (see Table 1). In this work, we do not explicitly model UV/LW radiation from BH accretion, given the limited understanding of the BH intrinsic SED in the early universe (see, e.g., J. E. Greene et al. 2026). We refer the reader to our previous work (S. Zhang et al. 2025a,b), and to a forthcoming study for a more comprehensive discussion of accretion feedback and the assumed seed mass.

motivated stellar evolution and feedback model, unlike the PBH_M5e7_fd005 run in which sink particles remain passive.

A metallicity threshold of $Z_{\text{th}} = 10^{-4} Z_{\odot}$ (with $Z_{\odot} = 0.02$) distinguishes Pop III and Population II (Pop II) star formation. Pop III stars follow a modified Larson IMF, where $dN/dM \propto M^{-\alpha} \exp(-M_{\text{cut}}^2/M^2)$, with $\alpha = 0.17$, $M_{\text{cut}}^2 = 20 M_{\odot}^2$, over the mass range $1 - 150 M_{\odot}$ (J. Jaacks et al. 2018), whereas a Chabrier IMF with a mass range of $0.08 - 100 M_{\odot}$ is assumed for Pop II stars (J. Jaacks et al. 2019). Each stellar particle (Pop III or Pop II) has a mass of $\simeq 600 M_{\odot}$. For Pop III, this mass corresponds to the typical mass of Pop III star clusters formed along the standard H_2 -cooling pathway (e.g., A. Stacy & V. Bromm 2013; S. Hirano & V. Bromm 2017; B. Liu et al. 2021, 2024).

Stellar feedback includes ionization heating, photo-dissociation of H_2 by Lyman-Werner (LW) radiation, thermal energy injection and metal enrichment from supernovae (J. Jaacks et al. 2018, 2019). The LW radiation field is computed based on both the global star formation rate density and local contributions from stellar particles (B. Liu & V. Bromm 2020b), assuming an optically thin regime while accounting for self-shielding¹². Reionization heating of the intergalactic medium (IGM) is modeled through a uniform global UV background with a characteristic self-shielding scale of ~ 1 kpc, based on the photoionization rate calculated by C.-A. Faucher-Giguère et al. (2009). The supernova (SN) feedback model follows the implementation of J. Jaacks et al. (2019), in which each stellar particle injects thermal energy, metals, and momentum into the surrounding gas based on IMF-averaged yields. For a typical stellar particle of mass $m_{\star} \simeq 600 M_{\odot}$, Pop III explosions release of order $\sim 7 \times 10^{51}$ erg with metal yields $\sim 39 M_{\odot}$, while Pop II particles contribute $\sim 6.7 \times 10^{51}$ erg and $\sim 10 M_{\odot}$ of metals, with lifetimes of ~ 3 and ~ 10 Myr, respectively. The resulting SN bubbles expand to characteristic radii of ~ 650 pc. A detailed description of the adopted parameters and their derivation can be found in Table 1 of B. Liu & V. Bromm (2020a) and in the feedback model presented by J. Jaacks et al. (2018, 2019).

3. RESULTS

With the stellar feedback recipes described in Section 2, we now analyze the resulting PBH simulation runs, comparing to previous work¹³ that did not include the full feedback physics. To study the synergy between

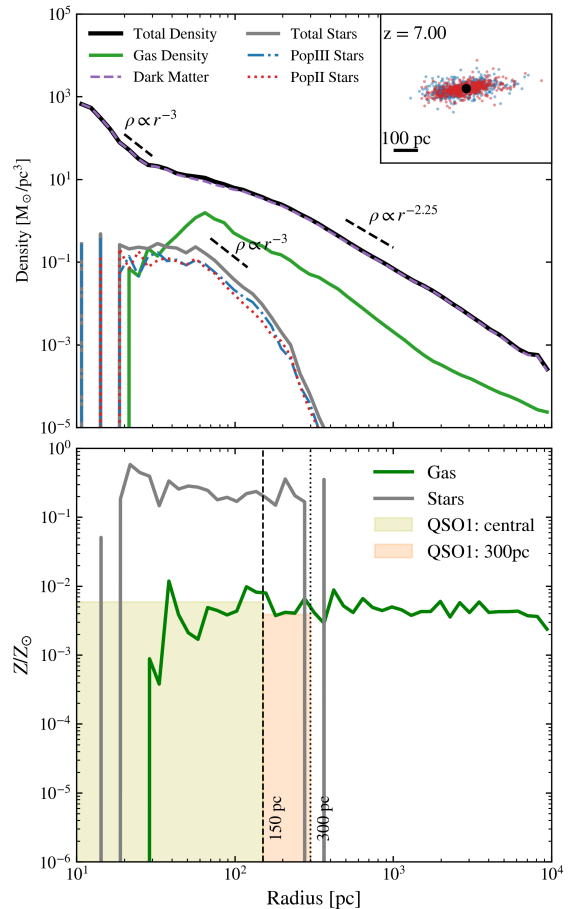


Figure 1. Matter density and metallicity profiles around the central BH at $z = 7$. Shown are the spherically averaged density and metallicity profiles from the final snapshot of the PBH_SF_M5e7_fd005 run. **Top:** Density of total matter (black), gas (green), dark matter (purple dashed), total stellar content (gray), Pop III stars (blue dashed-dotted), and Pop II stars (red dotted) vs. radius. Dashed black lines illustrate select power-law forms that match the simulated density profiles at certain parts. The inset shows the projected spatial distribution of Pop III (blue) and Pop II (red) stars relative to the central PBH (black circle), with a scale as indicated. **Bottom:** Radial metallicity profile for gas (green) and stars (grey), expressed in units of solar metallicity Z_{\odot} . Shaded regions indicate the observed metallicity constraints for Abell 2744-QSO1 within ~ 150 pc (yellow) and ~ 300 pc (orange) apertures (R. Maiolino et al. 2025). The simulated system exhibits a steep inner density profile and maintains subsolar gas metallicity throughout the central ~ 300 pc, in agreement with the properties inferred for QSO1.

stellar and BH feedback, metal enrichment, and gas outflow, we first track the star formation history (SFH) and the assembly of galaxies in Section 3.1, followed by a discussion of the metal enrichment history in Section 3.2.

¹² Here we do not consider LW radiation from the central BH (explored in S. Zhang et al. 2025a,b).

¹³ Also see the appendix in R. Maiolino et al. (2025).

3.1. Star Formation History

In *S. Zhang et al. (2025a)*, a BH seed of $10^6 M_\odot$ was placed at the center of the simulation box (with $L = 0.25 h^{-1} \text{Mpc}$), accelerating structure formation and seeding a $\sim 10^8 M_\odot$ halo by the termination redshift $z \sim 9$. When a fiducial feedback efficiency of $\epsilon_r = 0.005$ was assumed, star formation commenced at $z \sim 30$, and the BH growth remained modest ($\Delta m_{\text{BH}}/m_{\text{BH}} \lesssim 5\%$) by $z \sim 9$. In contrast, the present work embeds a much heavier initial seed of $5 \times 10^7 M_\odot$, resulting in a halo that is ~ 50 times more massive at the same redshift¹⁴ and providing a substantially larger gas reservoir available for accretion and star formation. At the same time, the rate of energy injection from BH accretion feedback scales as $\delta E_{\bullet, \text{inject}}/\delta t = \epsilon_{\text{EM}} \dot{m}_{\text{BH}} c^2 \propto m_{\text{BH}}^2$, implying that the more massive seed both consumes gas more rapidly and injects significantly greater energy into the surrounding medium than the $10^6 M_\odot$ case.

In this study, for both `PBH_M5e7_fd005` and `PBH_SF_M5e7_fd005`, the BH accretes at $\sim 1 - 10\%$ of the Eddington rate, in good agreement with the Eddington ratio $\sim 0.01 - 0.03$ of Abell 2744-QSO1 inferred by JWST. In our simulations, the BH spends roughly half of its time accreting within this range (see Fig. 2), ultimately reaching a final mass of $\sim 6 \times 10^7 M_\odot$ by $z = 7$. This strong feedback delays the onset of star formation until $z \lesssim 10$, despite the ample gas supply near the BH (see Table 1). We also present two additional cases, `PBH_SF_M5e7_fd0025` and `PBH_SF_M5e7_fd01`, where ϵ_r is reduced and enhanced by a factor of 2, respectively. We found that varying the feedback efficiency does not translate into a systematic shift of the star formation redshift, as both reducing and enhancing ϵ_r with respect to the fiducial choice leads to an earlier onset of star formation. Similarly, the central gas metallicity does not show any clear trend with ϵ_r , nor do we find a direct scaling with the total stellar mass formed. This reflects the stochastic/bursty nature of early star formation and metal mixing in PBH-seeded halos. Lowering ϵ_r leads to a higher time-averaged BH accretion rate, approximately following¹⁵ $\langle \dot{m}_{\text{BH}}/\dot{m}_{\text{edd}} \rangle \propto \epsilon_r^{-0.9}$, which partially compensates for the reduced feedback efficiency in maintaining a comparable time-averaged energy injection rate ($\propto \epsilon_r \dot{m}_{\text{BH}}$) across different simulations. As a result, the net heating of the gas only weakly depends on

ϵ_r , and the relevant effect is overwhelmed by stochasticity, such that changing ϵ_r does not necessarily decrease nor delay the onset of gas collapse in a particular halo.

We terminate the simulation at $z \sim 7$ and analyze the resulting stellar and gaseous structures. Figure 1 shows the radial distribution of stars, gas, dark matter, and metals surrounding the central PBH in the final snapshot of the `PBH_SF_M5e7_fd005` run, while Figure 2 presents the star formation histories for both the `PBH_M5e7_fd005` and `PBH_SF_M5e7_fd005` simulations. The density profile in Figure 1 exhibits a compact, approximately flat stellar core ($\rho \propto r^0$) within $r \lesssim r_{1/2} \sim 50$ pc, transitioning to a steep decline ($\rho \propto r^{-3}$) at $r \gtrsim 50$ pc where the gas component dominates. The overall dynamics, however, is governed by the dark matter halo, which develops a pronounced spike at $r \lesssim 30$ pc ($\rho \propto r^{-3}$) and a shallower profile at larger radii ($\rho \propto r^{-2.25}$ for $r \gtrsim 100$ pc). A similar structure is found in the `PBH_M5e7_fd005` run, though the absence of stellar feedback results in a more centrally concentrated stellar component. The total enclosed mass of dark matter, gas, and stars (as extended components) within 150 pc is comparable to the BH mass, generally consistent with the resolved kinematics¹⁶ of Abell 2744-QSO1 in observations (*I. Juodžbalis et al. 2025*).

Both simulations exhibit strongly episodic star formation. The initial burst is dominated by Pop III stars, reaching a peak rate of $\sim 1 M_\odot \text{yr}^{-1}$ before transitioning into Pop II star formation. In the `PBH_M5e7_fd005` run, this first burst lasts for ~ 50 Myr, which is followed by a ~ 50 Myr quiescent period before renewed star formation occurs. By $z \sim 7$, a stellar mass of $\sim 2 \times 10^7 M_\odot$ has formed near the PBH, close to the upper limit for Abell 2744-QSO1 placed by kinematic analysis. In contrast, the inclusion of stellar feedback in the `PBH_SF_M5e7_fd005` run drastically reduces the star formation efficiency: only a single ~ 50 Myr episode occurs, after which the system is quenched. By $z \sim 7$, a total stellar mass of $\sim 7.7 \times 10^5 M_\odot$ ($4.2 \times 10^5 M_\odot$ in Pop III and $3.5 \times 10^5 M_\odot$ in Pop II stars) has formed in the vicinity of the BH, assembling into a star cluster

¹⁴ The halo mass seeded by a PBH is expected to scale linearly with the PBH mass (*K. J. Mack et al. 2007*).

¹⁵ This empirical scaling is obtained from an extended suite of runs spanning multiple values of ϵ_r . For brevity, we do not show all runs in this paper, but the quoted fit is based on the full set.

¹⁶ We note that the mass ratio of the point source and the extended component inferred from observations depends on the density profile assumed for the latter. Besides, the dark-matter spike within $\lesssim 30$ pc cannot be separated from the BH point source observationally. Combining the spike with the BH as an effective central point mass, we obtain the simulated ratio $M_{\text{point}}/M_{\text{extended}} \approx 2.2$ (0.93) within 100 (150) pc, in agreement with the lack of significant contribution of an extended component in the resolved kinematics of QSO1, which indicates that $M_{\text{point}}/M_{\text{extended}} \gtrsim 2$, assuming a $n = 1$ Sérsic density profile of half mass radius 100 pc truncated at 300 pc for the extended component (*I. Juodžbalis et al. 2025*).

with a half-mass radius of $r_{1/2} \sim 55$ pc and a peak density exceeding $0.1 M_{\odot} \text{pc}^{-3}$. This simulated stellar mass is also consistent with the constraints ($M_{\star} \lesssim 10^6 M_{\odot}$) from optical and UV observations (X. Ji et al. 2025).

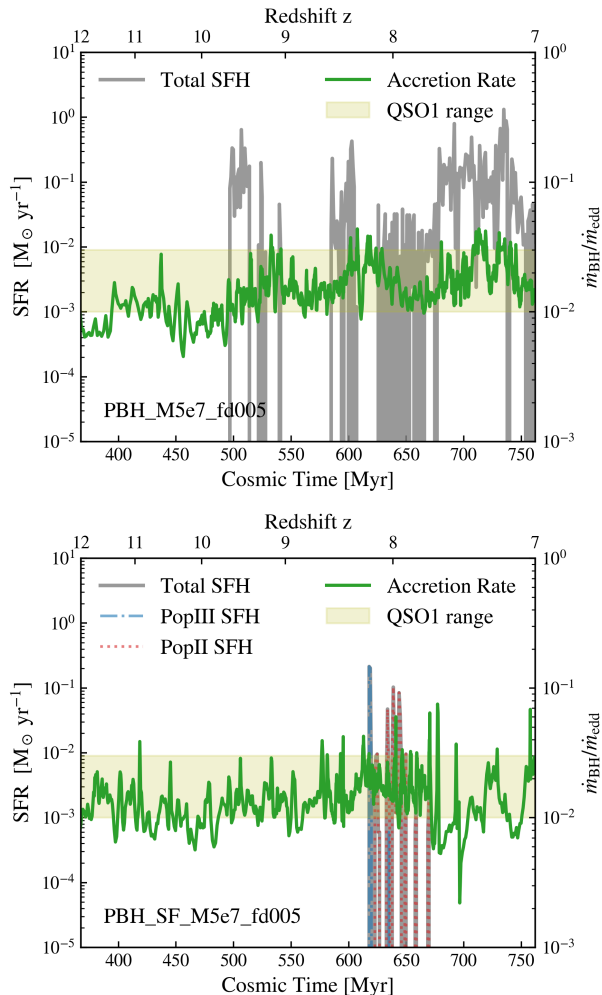


Figure 2. Combined BH accretion and star formation history. Shown are the BH accretion rates and star formation rates for the PBH_M5e7_fd005 and PBH_SF_M5e7_fd005 runs. **Top:** Accretion rate (green), expressed as a fraction of the Eddington limit, $\dot{m}_{\text{BH}}/\dot{m}_{\text{edd}}$, together with the total star formation rate (gray) within the vicinity of the PBH for the PBH_M5e7_fd005 run. Both quantities are shown as a function of cosmic time, with the corresponding redshift indicated on the upper axis. The shaded region (yellow) represents the accretion rate of Abell 2744-QSO1 inferred from observations as $\dot{m}_{\text{BH}}/\dot{m}_{\text{edd}} \sim 1 - 3\%$ (I. Juodžbalis et al. 2025). **Bottom:** Same as the top panel, but for the PBH_SF_M5e7_fd005 run. In this case, the total SFR (gray) is decomposed into its Pop III (blue dash-dotted) and Pop II (red dotted) components. In both simulations, BH accretion remains at $\sim 1 - 10\%$ of the Eddington level, while star formation occurs in short, bursty episodes regulated by BH feedback.

3.2. Metal Enrichment

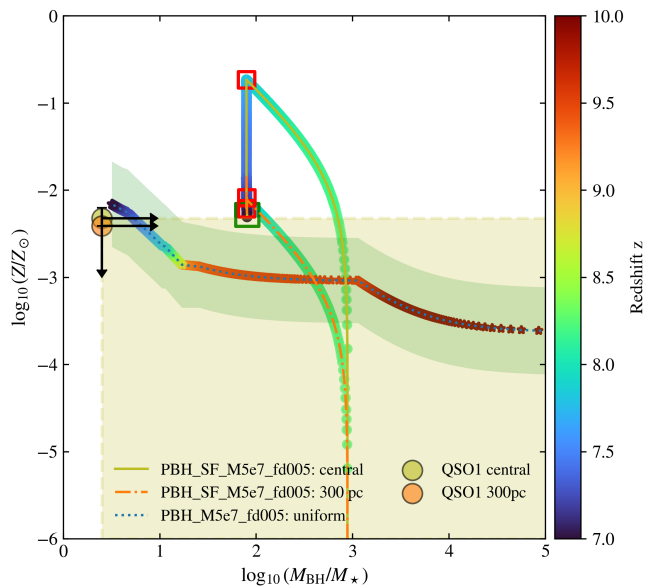


Figure 3. Metallicity evolution versus black-hole-to-stellar mass ratio in PBH-seeded galaxies. Shown are evolutionary tracks from two simulations with different feedback and spatial sampling: *uniform* metallicity measurements (stars with shaded band and dotted blue line) from the PBH_M5e7_fd005 run, and *central* (circles with olive solid line) and *300 pc* (circles with orange dot-dashed line) apertures from the PBH_SF_M5e7_fd005 run (mass-weighted). The color along each curve denotes redshift, from red ($z \sim 10$) to blue ($z \sim 7$), tracing metal enrichment over time. The green shaded region indicate model dispersion from analytical post-processing of the PBH_M5e7_fd005 run, while separate tracks show metallicities averaged over 0–150 pc (*central*) and 150–300 pc (*300 pc*) apertures. Square markers highlight the simulation snapshots from PBH_SF_M5e7_fd005: red squares indicate epochs that do not (or only partially) fall within the observationally allowed parameter space for Abell 2744-QSO1, while green squares mark snapshots consistent with the data^a. The yellow shaded region marks the allowed parameter space inferred for Abell 2744-QSO1, with its central (~ 150 pc) and extended (~ 300 pc) metallicity measurements shown as olive and orange points (R. Maiolino et al. 2025). By $z \approx 7$, the simulations naturally reach subsolar metallicities and high M_{BH}/M_{\star} ratios comparable to those inferred for QSO1.

^aNote that a few snapshots prior to star formation (not shown) are also found to satisfy the observed data.

In the PBH_SF_M5e7_fd005 run, metals are produced by both Pop III and Pop II stellar particles primarily during SN feedback events and are distributed, according to our numerical approach, to the gas particles within spherical SN bubbles. Once Pop III stars form within dense gas clouds, their short lifetimes (~ 3 Myr) rapidly enrich the local environment, elevating the local

metallicity above the critical threshold ($Z/Z_{\odot} \gtrsim 10^{-4}$) and triggering the subsequent formation of Pop II stars, as shown in the star formation history in Figure 2. The formation of these dense gas clouds around the PBH simultaneously enhances the accretion rate by a factor of $\sim 10\times$, as evidenced by the correlation between the early SFR burst and the elevated accretion activity in the same figure. During this efficient accretion phase, powerful outflows driven by BH thermal feedback expel metal-enriched gas from the central region, suppressing further star formation while the system continues to accrete pristine, neutral gas from the IGM. This continuous exchange between enriched outflows and pristine inflows drives down the average gas metallicity in the BH’s vicinity. The resulting evolution of metallicity as a function of the black-hole-to-stellar mass ratio is shown in Figure 3.

The PBH_M5e7_fd005 and PBH_SF_M5e7_fd005 runs exhibit similar global enrichment trends but differ in spatial and temporal detail. Prior to the onset of star formation ($z \gtrsim 10$), both systems remain essentially pristine, with metallicities below $10^{-6} Z_{\odot}$. Once star formation begins at $z \lesssim 10$, Pop III and subsequently Pop II stars form rapidly in compact clusters, while supernovae efficiently enrich the surrounding gas. In the PBH_SF_M5e7_fd005 run, the central region ($r < 150$ pc) enriches most efficiently, reaching $Z/Z_{\odot} \sim 10^{-1}$ by $z \sim 7.8$, while the outer region (150–300 pc) attains lower values at $Z/Z_{\odot} \sim 10^{-2}$. Between $z \sim 7$ and 8, strong BH-driven outflows remove enriched gas from the nucleus and suppress further star formation, lowering the average metallicity to levels consistent with Abell 2744–QSO1. The broadened track in Figure 3 shows the metallicity evolution inferred from post-processing the PBH_M5e7_fd005 run, where metallicities are averaged over the full outflow region. The broadening reflects the range of possible metal yields per unit stellar mass from different IMFs, following the methodology of R. Maiolino et al. (2025). Because this estimate averages over a much larger outflow region, the resulting metallicities are lower due to dilution by metal-poor gas. Overall, both simulations reproduce subsolar metallicities and the extreme M_{BH}/M_{\star} ratios observed by JWST, supporting a picture in which PBH-driven feedback regulates early star formation and chemical enrichment. Abell 2744–QSO1, as observed by JWST, may correspond either to the simulated system during or just prior to its initial starburst at $z \gtrsim 9$, or to a brief post-quenching phase near $z \sim 7$. Our simulations suggest that strong BH feedback can significantly delay the onset of star formation (see also S. Zhang et al. 2025a), and that JWST may be capturing an early evolutionary

stage of a PBH-seeded system, where the cosmic conditions at $z \sim 7$ remain similar to those simulated here at $z \sim 9$.

4. LIMITATION AND CAVEATS

Before discussing the broader implications of our PBH-seeded scenario, we note several subtleties in comparing our simulations with the observed dynamical constraints of Abell 2744–QSO1. The inferred point-to-extended mass ratio $M_{\text{point}}/M_{\text{extended}} \gtrsim 2$ reported by I. Juodžbalis et al. (2025) is sensitive to the assumed density profile of the extended component. In our simulations, the steep dark-matter spike formed within ~ 30 pc of the PBH is observationally indistinguishable from the unresolved BH itself; combining these components increases the effective central mass and yields point-to-extended mass ratios broadly within the allowed range for QSO1. Reproducing the observed rotation curve (I. Juodžbalis et al. 2025, see their fig. 1) within 1σ , however, requires lowering the central dark matter density (within ~ 150 pc) of the PBH-seeded dark-matter halo by a factor of ~ 2 –5.

While our current simulations capture the key physical processes linking PBH accretion, stellar feedback, and metal enrichment, several simplifications, although not drastically changing our conclusions, warrant further exploration in future works:

- Similar to S. Zhang et al. (2025a), our physical treatment of the PBH seed remains idealized. A single PBH seed is placed in an isolated box, neglecting potentially important effects such as an extended PBH mass function, PBH clustering, or mergers with forming galaxies. A broader PBH mass spectrum could alter small-scale structure formation (e.g., M. S. Delos et al. 2024), while clustering or early mergers may enhance gas inflow, BH growth, and star formation by supplying additional cold material (see a review of dual and binary SMBHs in A. De Rosa et al. 2019). Future work will explore a wider range of PBH masses, spatial configurations, simulation box sizes, and accretion prescriptions to quantify their impact on early SMBH–galaxy coevolution.
- A related limitation concerns our modeling of the dark matter component. In the present simulations, the PBH grows within collisionless PDM that does not undergo annihilation, self-interactions, or capture by the central PBH. As a result, the halo develops and maintains a steep inner cusp in PBH_SF_M5e7_fd005 (as shown in Figure 1). This profile is qualitatively consistent with

analytic expectations for the DM profile around a central compact object under adiabatic dynamical evolution (e.g., [D. Merritt 2004](#)). In mixed dark matter scenarios, however, the long-term evolution of the cusp may differ: annihilation can flatten the inner density profile, while PBH–DM capture or dynamical heating can remove dark matter from the center. In our simulations, the formation and evolution of PDM density spikes are related to both the density perturbations developed around the PBH during the radiation-dominated epoch (see, e.g., [S. M. Boucenna et al. 2018](#); [B. Carr et al. 2021c](#), also captured by the initial conditions of our simulations) and the subsequent infall of gas towards the center throughout the cosmic history. The interplay of these processes is still not fully understood. Capturing these processes and comparing to analytical predictions requires a more sophisticated treatment of dark matter microphysics, its interaction with baryons, and BH accretion feedback, which we leave for future work.

- Modeling stellar feedback in PBH-seeded systems is intrinsically complex, involving the interplay of radiative heating, SN explosions, and black-hole–driven outflows. In the present implementation, SN feedback is treated in a subgrid manner: each stellar particle releases metals and injects thermal energy into its surroundings at the end of its life. Metals are distributed uniformly in SN bubbles. However, this treatment neglects spatial inhomogeneities and small-scale turbulent mixing during enrichment (e.g., [J. S. Ritter et al. 2015](#)). As a result, it may underestimate local metallicity variations by overestimating the efficiency of chemical homogenization within the ISM (e.g., [R. Sarmiento & E. Scannapieco 2022](#); [U. P. Steinwandel et al. 2025](#)). Incorporating explicit metal-diffusion models and (sub-grid) turbulence-driven mixing prescriptions would yield a more physically accurate representation of early chemical enrichment in PBH-seeded galaxies.
- Our simulations assume BH feedback is purely thermal. However, at later stages, effects such as radiation pressure, mechanical winds, or jet-driven feedback may become important (see the review by [K. Inayoshi et al. 2020](#)). These processes can transport metal-enriched gas into the circumgalactic medium more efficiently. A more complete treatment that couples radiative transfer, kinetic feedback, and a multiphase ISM will

therefore be essential for capturing the full range of SMBH-driven regulation in early galaxies.

In this work, we focus on a proof-of-concept demonstration showing that a massive PBH seed can reproduce the observed properties of Abell 2744–QSO1. If one assumes that the entire JWST “little red dot” population originated from a similar PBH-seeded pathway, then using a measured number density of $\sim 4 \times 10^{-4} \text{ cMpc}^{-3}$ at $6.5 < z < 8.5$ for a rough estimate (e.g., see table 2 in [V. Kokorev et al. 2024](#)) would imply an upper limit on the density fraction of $5 \times 10^7 M_{\odot}$ PBH seeds of $f_{\text{PBH}} \lesssim 3.2 \times 10^{-7}$, much smaller than the existing constraints from dynamical effects and also below typical CMB heating/early-accretion limits (see, e.g., Sec. III.E of [B. Carr et al. 2021b](#))¹⁷. We note, however, that several recent studies have proposed alternative formation channels for LRDs and QSO1-like systems (e.g., [Y. Lu et al. \(2024\)](#); [W. Qin et al. \(2025\)](#); [F. Jiang et al. \(2026\)](#); [V. De Luca et al. \(2025\)](#), and see section 7 in [\(R. Maiolino et al. 2025\)](#)). Like our study, most of these works remain at the proof-of-concept stage and lack the follow-up numerical modeling required for a quantitative comparison across scenarios. A systematic assessment of competing pathways—spanning population statistics, chemical enrichment histories, environmental/clustering signatures, and multi-wavelength diagnostics—will therefore require substantial future work.

5. CONCLUSION

Our simulations reveal a plausible formation pathway for the JWST source Abell 2744–QSO1 within a PBH-seeded scenario. Beginning shortly after the recombination epoch, a massive PBH accelerates the assembly of structure and rapidly accretes the baryons funneled into its seed halo. However, the associated accretion feedback injects substantial thermal energy into the surrounding gas, delaying its cooling and the subsequent onset of star formation. Only once sufficient gas has accumulated and condensed in the potential well does a brief but intense episode of star formation occur in conjunction with enhanced BH accretion. As the ac-

¹⁷ For $30 M_{\odot} < M_{\text{PBH}} \lesssim 10^4 M_{\odot}$, a commonly used approximate scaling for the CMB heating/early-accretion limit is $f_{\text{PBH}} \lesssim (M_{\text{PBH}}/30 M_{\odot})^{-2}$, with a high-mass flattening at the level of $f_{\text{PBH}} \lesssim 10^{-5}$ under Eddington-limited accretion (see related treatments in [M. Ricotti et al. 2008](#); [Y. Ali-Haïmoud & M. Kamionkowski 2017](#)). On the other hand, CMB μ -distortion constraints tightly limit PBHs at this mass scale ([T. Nakama et al. 2018](#); [D. Hooper et al. 2024](#); [V. De Luca et al. 2025](#)), but these bounds assume Gaussian primordial fluctuations; non-Gaussianity or alternative formation scenarios can substantially weaken them (see, e.g., section II in [A. Escriv a et al. 2024](#)).

cretion rate rises, feedback from the central BH quickly becomes the dominant energy source, heating and expelling gas from the inner regions. This self-regulated phase quenches further star formation and suppresses additional metal enrichment, while powerful outflows redistribute and dilute metals throughout the ISM and circumgalactic medium.

The resulting system—whether observed immediately prior to star formation or shortly after the initial burst—naturally exhibits both low metallicity and an extreme black-hole-to-stellar mass ratio, reproducing the key properties of Abell 2744–QSO1 (as shown in Table 2). Moreover, the predicted PBH accretion rates, primarily regulated by BH feedback in our simulations, are consistent with the value inferred from observations. Early dominance of BH feedback thus provides a compelling physical explanation for the compact, metal-poor, BH-dominated systems uncovered by *JWST*.

Distinguishing observationally between a dense, star-free gas cocoon and a compact stellar cluster surrounding a primordial seed will require detailed modeling of the emergent spectral energy distribution (SED), including signatures of massive star formation, nebular line emission, and reprocessed radiation. In practice, however, these phases may be difficult to separate, since the central BH is enshrouded by dense metal-poor gas in both scenarios and the stellar component in our model is subdominant. It is also plausible that *JWST* may capture such systems during the brief, bursty star-formation episodes associated with enhanced BH accretion, as a natural outcome of PBH-regulated growth. Future work will incorporate radiative-transfer tools such as CLOUDY (M. Chatzikos et al. 2023) to generate self-consistent SEDs and mock observations, allowing more robust predictions for observational diagnostics. Ad-

ditional simulations in cosmological environments that permit PBH clustering, interactions, and early mergers will further enable a more complete characterization of the diversity of early SMBH–host galaxy co-evolution pathways. In parallel, future *JWST* ultra-deep surveys will be crucial for establishing a statistical census of LRDs. By increasing the number of spatially resolved, high-signal-to-noise detections of low-metallicity, BH-dominated systems, such surveys will enable population-level diagnostics such as number-density estimates, the distribution of M_{BH}/M_* , spatial metallicity gradients, and the fraction of sources exhibiting sub-Eddington accretion. These trends will provide key leverage for distinguishing PBH seeds from alternative formation pathways (see e.g., W. Qin et al. 2025; J. Jeon et al. 2025b), which predict different duty cycles, enrichment histories, and host-environment signatures.

ACKNOWLEDGMENTS

We acknowledge fruitful discussions with Priyamvada Natarajan, Fangzhou Jiang, Kohei Inayoshi, and Bar-mak Shams Es Haghi and within Mike Boylan-Kolchin’s group. The authors acknowledge the Texas Advanced Computing Center (TACC) for providing HPC resources under allocation AST23026. BL gratefully acknowledges the funding of the Royal Society University Research Fellowship and the Deutsche Forschungsgemeinschaft (DFG, German Research Foundation) under Germany’s Excellence Strategy EXC 2181/1 - 390900948 (the Heidelberg STRUCTURES Excellence Cluster).

Facilities: Lonestar6 and Stampede3 (TACC)

Software: astropy (Astropy Collaboration et al. 2013, 2018, 2022), Colossus (B. Diemer 2018)

REFERENCES

- Afshordi, N., McDonald, P., & Spergel, D. N. 2003, ApJL, 594, L71, doi: [10.1086/378763](https://doi.org/10.1086/378763)
- Agarwal, B., Dalla Vecchia, C., Johnson, J. L., Khochfar, S., & Paardekooper, J.-P. 2014, MNRAS, 443, 648, doi: [10.1093/mnras/stu1112](https://doi.org/10.1093/mnras/stu1112)
- Alexander, T., & Natarajan, P. 2014, Science, 345, 1330, doi: [10.1126/science.1251053](https://doi.org/10.1126/science.1251053)
- Ali-Haïmoud, Y., & Kamionkowski, M. 2017, PhRvD, 95, 043534, doi: [10.1103/PhysRevD.95.043534](https://doi.org/10.1103/PhysRevD.95.043534)
- Astropy Collaboration, Robitaille, T. P., Tollerud, E. J., et al. 2013, A&A, 558, A33, doi: [10.1051/0004-6361/201322068](https://doi.org/10.1051/0004-6361/201322068)
- Astropy Collaboration, Price-Whelan, A. M., Sipőcz, B. M., et al. 2018, AJ, 156, 123, doi: [10.3847/1538-3881/aabc4f](https://doi.org/10.3847/1538-3881/aabc4f)
- Astropy Collaboration, Price-Whelan, A. M., Lim, P. L., et al. 2022, ApJ, 935, 167, doi: [10.3847/1538-4357/ac7c74](https://doi.org/10.3847/1538-4357/ac7c74)
- Begelman, M. C., Volonteri, M., & Rees, M. J. 2006, MNRAS, 370, 289, doi: [10.1111/j.1365-2966.2006.10467.x](https://doi.org/10.1111/j.1365-2966.2006.10467.x)
- Belotsky, K. M., Dokuchaev, V. I., Eroshenko, Y. N., et al. 2019, Eur. Phys. J. C, 79, 246, doi: [10.1140/epjc/s10052-019-6741-4](https://doi.org/10.1140/epjc/s10052-019-6741-4)
- Bernal, J. L., Raccanelli, A., Verde, L., & Silk, J. 2018, JCAP, 05, 017, doi: [10.1088/1475-7516/2018/05/017](https://doi.org/10.1088/1475-7516/2018/05/017)

Table 2. Comparison of key observed properties of Abell 2744–QSO1 (adapted from Table 2 in R. Maiolino et al. 2025) and the corresponding values from our PBH-seeded simulation (the PBH_SF_M5e7_fd005 run) snapshot at $z \simeq 7$.

Quantity	Observation (QSO1)	Simulation ($z \simeq 7$)
BH Mass, $M_{\text{BH}}([M_{\odot}])$	$\sim (2.5\text{--}10) \times 10^7$	$\sim 6 \times 10^7$
Stellar Mass, $M_{\star}([M_{\odot}])$	$\lesssim 2 \times 10^7$ (dynamics), $\sim 10^6$ (optical and UV)	$\sim 7.7 \times 10^5$
M_{BH}/M_{\star}	$\gtrsim 2$ (model dependent)	~ 80
Metallicity ($R < 150$ pc; $[Z/Z_{\odot}]$)	$\sim 10^{-2.23} - 10^{-2.44}$	$\sim 10^{-2.28}$
Metallicity (150 pc $< R < 300$ pc; $[Z/Z_{\odot}]$)	$\lesssim 10^{-2.41}$	$\sim 10^{-2.31}$
Eddington Ratio, f_{Edd}	$\sim 0.01\text{--}0.03$	~ 0.02

- Bogdán, Á., Goulding, A. D., Natarajan, P., et al. 2024, *Nature Astronomy*, 8, 126, doi: [10.1038/s41550-023-02111-9](https://doi.org/10.1038/s41550-023-02111-9)
- Boucenna, S. M., Kühnel, F., Ohlsson, T., & Visinelli, L. 2018, *JCAP*, 2018, 003, doi: [10.1088/1475-7516/2018/07/003](https://doi.org/10.1088/1475-7516/2018/07/003)
- Bromm, V., Coppi, P. S., & Larson, R. B. 2002, *ApJ*, 564, 23, doi: [10.1086/323947](https://doi.org/10.1086/323947)
- Bromm, V., & Loeb, A. 2003, *ApJ*, 596, 34, doi: [10.1086/377529](https://doi.org/10.1086/377529)
- Cappelluti, N., Hasinger, G., & Natarajan, P. 2022, *ApJ*, 926, 205, doi: [10.3847/1538-4357/ac332d](https://doi.org/10.3847/1538-4357/ac332d)
- Carr, B., Clesse, S., García-Bellido, J., & Kühnel, F. 2021a, *Physics of the Dark Universe*, 31, 100755, doi: [10.1016/j.dark.2020.100755](https://doi.org/10.1016/j.dark.2020.100755)
- Carr, B., Kohri, K., Sendouda, Y., & Yokoyama, J. 2021b, *Reports on Progress in Physics*, 84, 116902, doi: [10.1088/1361-6633/ac1e31](https://doi.org/10.1088/1361-6633/ac1e31)
- Carr, B., & Kühnel, F. 2020, *Annual Review of Nuclear and Particle Science*, 70, 355, doi: [10.1146/annurev-nucl-050520-125911](https://doi.org/10.1146/annurev-nucl-050520-125911)
- Carr, B., Kühnel, F., & Visinelli, L. 2021c, *MNRAS*, 506, 3648, doi: [10.1093/mnras/stab1930](https://doi.org/10.1093/mnras/stab1930)
- Carr, B., & Silk, J. 2018, *MNRAS*, 478, 3756, doi: [10.1093/mnras/sty1204](https://doi.org/10.1093/mnras/sty1204)
- Carr, B. J. 1975, *ApJ*, 201, 1, doi: [10.1086/153853](https://doi.org/10.1086/153853)
- Casanueva-Villarreal, C., Tissera, P. B., Padilla, N., et al. 2024, *A&A*, 688, A183, doi: [10.1051/0004-6361/202449650](https://doi.org/10.1051/0004-6361/202449650)
- Chatzikos, M., Bianchi, S., Camilloni, F., et al. 2023, *RMxAA*, 59, 327, doi: [10.22201/ia.01851101p.2023.59.02.12](https://doi.org/10.22201/ia.01851101p.2023.59.02.12)
- Colazo, P. E., Stasyszyn, F., & Padilla, N. 2024, *A&A*, 685, L8, doi: [10.1051/0004-6361/202449565](https://doi.org/10.1051/0004-6361/202449565)
- Dayal, P. 2024, *A&A*, 690, A182, doi: [10.1051/0004-6361/202451481](https://doi.org/10.1051/0004-6361/202451481)
- Dayal, P., & Maiolino, R. 2025, arXiv e-prints, arXiv:2506.08116, doi: [10.48550/arXiv.2506.08116](https://doi.org/10.48550/arXiv.2506.08116)
- De Luca, V., Del Grosso, L., Franciolini, G., et al. 2025, arXiv e-prints, arXiv:2512.19666, doi: [10.48550/arXiv.2512.19666](https://doi.org/10.48550/arXiv.2512.19666)
- De Luca, V., Franciolini, G., Pani, P., & Riotto, A. 2020, *JCAP*, 2020, 044, doi: [10.1088/1475-7516/2020/06/044](https://doi.org/10.1088/1475-7516/2020/06/044)
- De Luca, V., Franciolini, G., & Riotto, A. 2023, *PhRvL*, 130, 171401, doi: [10.1103/PhysRevLett.130.171401](https://doi.org/10.1103/PhysRevLett.130.171401)
- De Rosa, A., Vignali, C., Bogdanović, T., et al. 2019, *NewAR*, 86, 101525, doi: [10.1016/j.newar.2020.101525](https://doi.org/10.1016/j.newar.2020.101525)
- Delos, M. S., Rantala, A., Young, S., & Schmidt, F. 2024, *JCAP*, 2024, 005, doi: [10.1088/1475-7516/2024/12/005](https://doi.org/10.1088/1475-7516/2024/12/005)
- Diemer, B. 2018, *ApJS*, 239, 35, doi: [10.3847/1538-4365/aee8c](https://doi.org/10.3847/1538-4365/aee8c)
- Düchting, N. 2004, *PhRvD*, 70, 064015, doi: [10.1103/PhysRevD.70.064015](https://doi.org/10.1103/PhysRevD.70.064015)
- Escrivà, A. 2022, *Universe*, 8, 66, doi: [10.3390/universe8020066](https://doi.org/10.3390/universe8020066)
- Escrivà, A., Kühnel, F., & Tada, Y. 2024, in *Black Holes in the Era of Gravitational-Wave Astronomy*, ed. M. Arca Sedda, E. Bortolas, & M. Spera, 261–377, doi: [10.1016/B978-0-32-395636-9.00012-8](https://doi.org/10.1016/B978-0-32-395636-9.00012-8)
- Faucher-Giguère, C.-A., Lidz, A., Zaldarriaga, M., & Hernquist, L. 2009, *ApJ*, 703, 1416, doi: [10.1088/0004-637X/703/2/1416](https://doi.org/10.1088/0004-637X/703/2/1416)
- Furtak, L. J., Zitrin, A., Plat, A., et al. 2023, *ApJ*, 952, 142, doi: [10.3847/1538-4357/acdc9d](https://doi.org/10.3847/1538-4357/acdc9d)
- Galli, D., & Palla, F. 2013, *ARA&A*, 51, 163, doi: [10.1146/annurev-astro-082812-141029](https://doi.org/10.1146/annurev-astro-082812-141029)
- Goulding, A. D., Greene, J. E., Setton, D. J., et al. 2023, *ApJL*, 955, L24, doi: [10.3847/2041-8213/acf7c5](https://doi.org/10.3847/2041-8213/acf7c5)
- Greene, J. E., Labbe, I., Goulding, A. D., et al. 2024, *ApJ*, 964, 39, doi: [10.3847/1538-4357/ad1e5f](https://doi.org/10.3847/1538-4357/ad1e5f)
- Greene, J. E., Setton, D. J., Furtak, L. J., et al. 2026, *ApJ*, 996, 129, doi: [10.3847/1538-4357/ae1836](https://doi.org/10.3847/1538-4357/ae1836)
- Habouzit, M., Volonteri, M., Latif, M., Dubois, Y., & Peirani, S. 2016, *MNRAS*, 463, 529, doi: [10.1093/mnras/stw1924](https://doi.org/10.1093/mnras/stw1924)
- Hahn, O., & Abel, T. 2011, *MNRAS*, 415, 2101, doi: [10.1111/j.1365-2966.2011.18820.x](https://doi.org/10.1111/j.1365-2966.2011.18820.x)

- Hawking, S. 1971, *Monthly Notices of the Royal Astronomical Society*, 152, 75
- Hirano, S., & Bromm, V. 2017, *MNRAS*, 470, 898, doi: [10.1093/mnras/stx1220](https://doi.org/10.1093/mnras/stx1220)
- Hooper, D., Ireland, A., Krnjaic, G., & Stebbins, A. 2024, *JCAP*, 2024, 021, doi: [10.1088/1475-7516/2024/04/021](https://doi.org/10.1088/1475-7516/2024/04/021)
- Hopkins, P. F. 2015, *MNRAS*, 450, 53, doi: [10.1093/mnras/stv195](https://doi.org/10.1093/mnras/stv195)
- Inayoshi, K., Kashiyama, K., Li, W., et al. 2024, *ApJ*, 966, 164, doi: [10.3847/1538-4357/ad344c](https://doi.org/10.3847/1538-4357/ad344c)
- Inayoshi, K., Visbal, E., & Haiman, Z. 2020, *ARA&A*, 58, 27, doi: [10.1146/annurev-astro-120419-014455](https://doi.org/10.1146/annurev-astro-120419-014455)
- Inman, D., & Ali-Haïmoud, Y. 2019, *PhRvD*, 100, 083528, doi: [10.1103/PhysRevD.100.083528](https://doi.org/10.1103/PhysRevD.100.083528)
- Jaacks, J., Finkelstein, S. L., & Bromm, V. 2019, *MNRAS*, 488, 2202, doi: [10.1093/mnras/stz1529](https://doi.org/10.1093/mnras/stz1529)
- Jaacks, J., Thompson, R., Finkelstein, S. L., & Bromm, V. 2018, *MNRAS*, 475, 4396, doi: [10.1093/mnras/sty062](https://doi.org/10.1093/mnras/sty062)
- Jeon, J., Bromm, V., Liu, B., & Finkelstein, S. L. 2025a, *ApJ*, 979, 127, doi: [10.3847/1538-4357/ad9f3a](https://doi.org/10.3847/1538-4357/ad9f3a)
- Jeon, J., Liu, B., Bromm, V., & Finkelstein, S. L. 2023, *MNRAS*, 524, 176, doi: [10.1093/mnras/stad1877](https://doi.org/10.1093/mnras/stad1877)
- Jeon, J., Liu, B., Bromm, V., et al. 2025b, arXiv e-prints, arXiv:2508.14155, doi: [10.48550/arXiv.2508.14155](https://doi.org/10.48550/arXiv.2508.14155)
- Ji, X., Maiolino, R., Übler, H., et al. 2025, *MNRAS*, 544, 3900, doi: [10.1093/mnras/staf1867](https://doi.org/10.1093/mnras/staf1867)
- Jiang, F., Jia, Z., Zheng, H., et al. 2026, *ApJL*, 996, L19, doi: [10.3847/2041-8213/ae247a](https://doi.org/10.3847/2041-8213/ae247a)
- Johnson, J. L., & Bromm, V. 2006, *MNRAS*, 366, 247, doi: [10.1111/j.1365-2966.2005.09846.x](https://doi.org/10.1111/j.1365-2966.2005.09846.x)
- Juodžbalis, I., Marconcini, C., D'Eugenio, F., et al. 2025, arXiv e-prints, arXiv:2508.21748, doi: [10.48550/arXiv.2508.21748](https://doi.org/10.48550/arXiv.2508.21748)
- Kashlinsky, A. 2021, *PhRvL*, 126, 011101, doi: [10.1103/PhysRevLett.126.011101](https://doi.org/10.1103/PhysRevLett.126.011101)
- Kocevski, D. D., Finkelstein, S. L., Barro, G., et al. 2025, *ApJ*, 986, 126, doi: [10.3847/1538-4357/adbc7d](https://doi.org/10.3847/1538-4357/adbc7d)
- Kokorev, V., Caputi, K. I., Greene, J. E., et al. 2024, *ApJ*, 968, 38, doi: [10.3847/1538-4357/ad4265](https://doi.org/10.3847/1538-4357/ad4265)
- Kovács, O. E., Bogdán, Á., Natarajan, P., et al. 2024, *ApJL*, 965, L21, doi: [10.3847/2041-8213/ad391f](https://doi.org/10.3847/2041-8213/ad391f)
- Labbé, I., van Dokkum, P., Nelson, E., et al. 2023, *Nature*, 616, 266, doi: [10.1038/s41586-023-05786-2](https://doi.org/10.1038/s41586-023-05786-2)
- Labbe, I., Greene, J. E., Bezanson, R., et al. 2025, *ApJ*, 978, 92, doi: [10.3847/1538-4357/ad3551](https://doi.org/10.3847/1538-4357/ad3551)
- Larson, R. L., Finkelstein, S. L., Kocevski, D. D., et al. 2023, *ApJL*, 953, L29, doi: [10.3847/2041-8213/ace619](https://doi.org/10.3847/2041-8213/ace619)
- Leung, G. C. K., Finkelstein, S. L., Pérez-González, P. G., et al. 2025, *ApJ*, 992, 26, doi: [10.3847/1538-4357/adfcee](https://doi.org/10.3847/1538-4357/adfcee)
- Liu, B., & Bromm, V. 2020a, *MNRAS*, 497, 2839, doi: [10.1093/mnras/staa2143](https://doi.org/10.1093/mnras/staa2143)
- Liu, B., & Bromm, V. 2020b, *MNRAS*, 495, 2475, doi: [10.1093/mnras/staa1362](https://doi.org/10.1093/mnras/staa1362)
- Liu, B., & Bromm, V. 2022, *ApJL*, 937, L30, doi: [10.3847/2041-8213/ac927f](https://doi.org/10.3847/2041-8213/ac927f)
- Liu, B., & Bromm, V. 2023, arXiv e-prints, arXiv:2312.04085, doi: [10.48550/arXiv.2312.04085](https://doi.org/10.48550/arXiv.2312.04085)
- Liu, B., Gurian, J., Inayoshi, K., et al. 2024, *MNRAS*, 534, 290, doi: [10.1093/mnras/stae2066](https://doi.org/10.1093/mnras/stae2066)
- Liu, B., Meynet, G., & Bromm, V. 2021, *MNRAS*, 501, 643, doi: [10.1093/mnras/staa3671](https://doi.org/10.1093/mnras/staa3671)
- Liu, B., Zhang, S., & Bromm, V. 2022, *MNRAS*, 514, 2376, doi: [10.1093/mnras/stac1472](https://doi.org/10.1093/mnras/stac1472)
- Lodato, G., & Natarajan, P. 2006, *MNRAS*, 371, 1813, doi: [10.1111/j.1365-2966.2006.10801.x](https://doi.org/10.1111/j.1365-2966.2006.10801.x)
- Loeb, A., & Rasio, F. A. 1994, *ApJ*, 432, 52, doi: [10.1086/174548](https://doi.org/10.1086/174548)
- Lu, P., Takhistov, V., Gelmini, G. B., et al. 2021, *ApJL*, 908, L23, doi: [10.3847/2041-8213/abdcb6](https://doi.org/10.3847/2041-8213/abdcb6)
- Lu, Y., Picker, Z. S. C., & Kusenko, A. 2024, *PhRvD*, 109, 123016, doi: [10.1103/PhysRevD.109.123016](https://doi.org/10.1103/PhysRevD.109.123016)
- Mack, K. J., Ostriker, J. P., & Ricotti, M. 2007, *ApJ*, 665, 1277, doi: [10.1086/518998](https://doi.org/10.1086/518998)
- Maiolino, R., Scholtz, J., Curtis-Lake, E., et al. 2024, *A&A*, 691, A145, doi: [10.1051/0004-6361/202347640](https://doi.org/10.1051/0004-6361/202347640)
- Maiolino, R., Uebler, H., D'Eugenio, F., et al. 2025, arXiv e-prints, arXiv:2505.22567, doi: [10.48550/arXiv.2505.22567](https://doi.org/10.48550/arXiv.2505.22567)
- Matteri, A., Ferrara, A., & Pallottini, A. 2025, *A&A*, 701, A186, doi: [10.1051/0004-6361/202554728](https://doi.org/10.1051/0004-6361/202554728)
- Merritt, D. 2004, *PhRvL*, 92, 201304, doi: [10.1103/PhysRevLett.92.201304](https://doi.org/10.1103/PhysRevLett.92.201304)
- Meszaros, P. 1975, *A&A*, 38, 5
- Milosavljević, M., Bromm, V., Couch, S. M., & Oh, S. P. 2009, *ApJ*, 698, 766, doi: [10.1088/0004-637X/698/1/766](https://doi.org/10.1088/0004-637X/698/1/766)
- Nakama, T., Carr, B., & Silk, J. 2018, *PhRvD*, 97, 043525, doi: [10.1103/PhysRevD.97.043525](https://doi.org/10.1103/PhysRevD.97.043525)
- Napolitano, L., Castellano, M., Pentericci, L., et al. 2025, *ApJ*, 989, 75, doi: [10.3847/1538-4357/ade706](https://doi.org/10.3847/1538-4357/ade706)
- Natarajan, P., Pacucci, F., Ricarte, A., et al. 2024, *ApJL*, 960, L1, doi: [10.3847/2041-8213/ad0e76](https://doi.org/10.3847/2041-8213/ad0e76)
- O'Brennan, H., Regan, J. A., Brennan, J., et al. 2025, *The Open Journal of Astrophysics*, 8, 88, doi: [10.33232/001c.141953](https://doi.org/10.33232/001c.141953)
- Pacucci, F., Nguyen, B., Carniani, S., Maiolino, R., & Fan, X. 2023, *ApJL*, 957, L3, doi: [10.3847/2041-8213/ad0158](https://doi.org/10.3847/2041-8213/ad0158)
- Planck Collaboration, Aghanim, N., Akrami, Y., et al. 2020, *A&A*, 641, A6, doi: [10.1051/0004-6361/201833910](https://doi.org/10.1051/0004-6361/201833910)

- Qin, W., Kumar, S., Natarajan, P., & Weiner, N. 2025, arXiv e-prints, arXiv:2506.13858, doi: [10.48550/arXiv.2506.13858](https://doi.org/10.48550/arXiv.2506.13858)
- Ricotti, M. 2007, ApJ, 662, 53, doi: [10.1086/516562](https://doi.org/10.1086/516562)
- Ricotti, M., Ostriker, J. P., & Mack, K. J. 2008, ApJ, 680, 829, doi: [10.1086/587831](https://doi.org/10.1086/587831)
- Ritter, J. S., Sluder, A., Safraneck-Shrader, C., Milosavljević, M., & Bromm, V. 2015, MNRAS, 451, 1190, doi: [10.1093/mnras/stv982](https://doi.org/10.1093/mnras/stv982)
- Sarmiento, R., & Scannapieco, E. 2022, ApJ, 935, 174, doi: [10.3847/1538-4357/ac815c](https://doi.org/10.3847/1538-4357/ac815c)
- Smith, A., & Bromm, V. 2019, Contemporary Physics, 60, 111, doi: [10.1080/00107514.2019.1615715](https://doi.org/10.1080/00107514.2019.1615715)
- Springel, V. 2005, MNRAS, 364, 1105, doi: [10.1111/j.1365-2966.2005.09655.x](https://doi.org/10.1111/j.1365-2966.2005.09655.x)
- Stacy, A., & Bromm, V. 2013, MNRAS, 433, 1094, doi: [10.1093/mnras/stt789](https://doi.org/10.1093/mnras/stt789)
- Steinwandel, U. P., Rennehan, D., Orr, M. E., Fielding, D. B., & Kim, C.-G. 2025, ApJ, 991, 16, doi: [10.3847/1538-4357/adf283](https://doi.org/10.3847/1538-4357/adf283)
- Su, B.-Y., Li, N., & Feng, L. 2023, arXiv e-prints, arXiv:2306.05364, doi: [10.48550/arXiv.2306.05364](https://doi.org/10.48550/arXiv.2306.05364)
- Takhistov, V., Lu, P., Gelmini, G. B., et al. 2022, JCAP, 2022, 017, doi: [10.1088/1475-7516/2022/03/017](https://doi.org/10.1088/1475-7516/2022/03/017)
- Taylor, A. J., Finkelstein, S. L., Kocevski, D. D., et al. 2025, ApJ, 986, 165, doi: [10.3847/1538-4357/add15b](https://doi.org/10.3847/1538-4357/add15b)
- Zel'dovich, Y. B., & Novikov, I. D. 1967, Soviet Ast., 10, 602
- Zhang, B., Feng, W.-X., & An, H. 2025, arXiv e-prints, arXiv:2507.07171, doi: [10.48550/arXiv.2507.07171](https://doi.org/10.48550/arXiv.2507.07171)
- Zhang, S., Bromm, V., & Liu, B. 2024a, ApJ, 975, 139, doi: [10.3847/1538-4357/ad7b0d](https://doi.org/10.3847/1538-4357/ad7b0d)
- Zhang, S., Liu, B., & Bromm, V. 2024b, MNRAS, 528, 180, doi: [10.1093/mnras/stad3986](https://doi.org/10.1093/mnras/stad3986)
- Zhang, S., Liu, B., & Bromm, V. 2025, PHANTOM: Primordial black Holes And Nonlinear perturbations for siMulations, Zenodo, doi: [10.5281/zenodo.17025634](https://doi.org/10.5281/zenodo.17025634)
- Zhang, S., Liu, B., & Bromm, V. 2025b, ApJ, 992, 136, doi: [10.3847/1538-4357/ae061c](https://doi.org/10.3847/1538-4357/ae061c)
- Zhang, S., Liu, B., Bromm, V., et al. 2025a, ApJ, 987, 185, doi: [10.3847/1538-4357/adddb4](https://doi.org/10.3847/1538-4357/adddb4)
- Ziparo, F., Gallerani, S., Ferrara, A., & Vito, F. 2022, MNRAS, 517, 1086, doi: [10.1093/mnras/stac2705](https://doi.org/10.1093/mnras/stac2705)